USCAP

Check for updates

ARTICLE

Identification of novel *SSX1* fusions in synovial sarcoma

Akihiko Yoshida [1,2✉], Yasuhito Arai [3], Kaishi Satomi [1], Takashi Kubo[4,5], Eijitsu Ryo[6], Yuko Matsushita[7,12], Natsuko Hama[3], Kazuki Sudo[2,8], Motokiyo Komiyama[2,9], Yasushi Yatabe [1,6], Tatsuhiro Shibata[3], Hitoshi Ichikawa [5,10], Koichi Ichimura [7,12], Akira Kawai[2,11] and Taisuke Mori [1,6]

Synovial sarcoma is characterized by variable epithelial differentiation and specific *SS18-SSX* gene fusions. The diagnosis is primarily based on phenotype, but fusion gene detection is increasingly being considered indispensable, with *SS18* break-apart fluorescence in situ hybridization (FISH) being favored in many laboratories. However, *SS18* FISH assay produces negative or atypical results in a minority of cases, leaving uncertainties in diagnosis and management. Here, we analyzed this challenging subset of *SS18* FISH-negative/atypical synovial sarcoma using RNA sequencing and monoclonal antibodies that recognize SS18-SSX and the SSX C-terminus. Among 99 synovial sarcoma cases that were previously subjected to *SS18* break-apart FISH, eight cases were reported as negative and three cases were indeterminate, owing to atypical signal patterns. Three of these 11 tumors (two monophasic and one biphasic) harbored novel *EWSR1-SSX1* fusions, were negative for SS18-SSX staining, and were positive for SSX C-terminus staining. One monophasic tumor harbored a novel *MN1-SSX1* fusion, and showed negative SS18-SSX expression and positive SSX C-terminus staining. Another monophasic tumor carried an *SS18L1-SSX1* fusion, and was weakly positive for SS18-SSX, while SMARCB1 expression was reduced. The presence of these novel and/or rare fusions was confirmed using RT-PCR and Sanger sequencing. *EWSR1-SSX1* was further validated by *EWSR1* FISH assay. The remaining six tumors (five monophasic and one biphasic) showed strong SS18-SSX expression, and RNA sequencing successfully performed in three cases identified canonical *SS18-SSX2* fusions. Based on a DNA methylation-based unsupervised clustering, the tumors with *EWSR1-SSX1* and *SS18L1-SSX1* clustered with synovial sarcoma, while the *MN1-SSX1*-positive tumor was not co-clustered despite classic histology and immunoprofile. In summary, we discovered novel and rare *SSX1* fusions to non-*SS18* genes in synovial sarcoma. The expanded genetic landscape carries significant diagnostic implications and advances our understanding of the oncogenic mechanism.

INTRODUCTION

Synovial sarcoma (SS) accounts for up to 10% of soft tissue sarcomas, and often affects the deep soft tissues of young adults. The monophasic spindle cell subtype consists of dense fascicles of uniform spindle cells, whereas epithelial glands and nests are present in the biphasic subtype. A poorly differentiated pattern is defined by the presence of mitotically active, highly atypical round or spindle cells. Immunohistochemically, SS often shows scattered cytokeratin and more widespread epithelial membrane antigen (EMA) expression, along with intense diffuse TLE1 expression in >90% of cases[1], while CD34 expression is typically negative[2]. Occasional BCOR expression is a confusing finding in the differential diagnosis of sarcoma with BCOR genetic abnormalities[3]. SS is genetically characterized by *SS18* gene fusions including *SS18-SSX1*, *SS18-SSX2*, and *SS18-SSX4*. The alternative fusions *SS18L1-SSX1* and *SS18-NEDD4* have been reported in two and one cases, respectively[3–5]. SS18-SSX fusion oncoprotein binds

to the BAF (SWI/SNF) complex and causes displacement of native SS18 and eviction of SMARCB1 (also known as INI1 and BAF47)[6]. Reduced immunohistochemical expression of SMARCB1 is accordingly observed in up to 90% of SS samples[7,8].

The diagnosis of SS is primarily based on histomorphology and immunophenotype. However, molecular genetic detection of *SS18-SSX* fusion is increasingly considered indispensable. The fusion can be detected by various methods, including reverse transcription polymerase chain reaction (RT-PCR) and fluorescence in situ hybridization (FISH). *SS18* break-apart FISH is favored by most laboratories, as it is readily applicable to a single thin FFPE section with good morphological control. As a result, *SS18* break-apart FISH is often considered the gold standard of SS diagnosis. However, FISH is not entirely sensitive. In previous studies using >20 cases and a commercially available *SS18* break-apart FISH probe, the sensitivity of the *SS18* FISH assay was 82–97%[9–13], with most studies reporting a rate less than 90%[10,12,13], which is

¹Department of Diagnostic Pathology, National Cancer Center Hospital, Tokyo, Japan. ²Rare Cancer Center, National Cancer Center Hospital, Tokyo, Japan. ³Division of Cancer Genomics, National Cancer Center Research Institute, Tokyo, Japan. ⁴Department of Laboratory Medicine, National Cancer Center Hospital, Tokyo, Japan. ⁵Department of Clinical Genomics, National Cancer Center Research Institute, Tokyo, Japan. ⁶Division of Molecular Pathology, National Cancer Center Research Institute, Tokyo, Japan. ⁷Division of Brain Tumor Translational Research, National Cancer Center Research Institute, Tokyo, Japan. ⁸Department of Medical Oncology, National Cancer Center Hospital, Tokyo, Japan. ⁹Department of Urology, National Cancer Center Hospital, Tokyo, Japan. ¹⁰Division of Translational Genomics, Exploratory Oncology Research and Clinical Trial Center, National Cancer Center, Tokyo, Japan. ¹¹Department of Musculoskeletal Oncology, National Cancer Center Hospital, Tokyo, Japan. ¹²Present address: Department of Brain Disease Translational Research, Juntendo University Faculty of Medicine, Tokyo, Japan. ✉email: akyoshid@ncc.go.jp

generally lower than that of RT-PCR assays[9,10,12,14]. Even taking into account an uncommon but accepted positive pattern of isolated *SS18* 5′ signal predominance[9,10,15], a significant minority of SS shows negative or atypical/uninterpretable signals. In our experience, we have occasionally observed sarcomas that phenotypically match with SS, yet fail to demonstrate evidence of *SS18* rearrangement by FISH. While some of these cases received definitive diagnosis based on classic phenotypes including TLE1 positivity and reduced SMARCB1 expression, other cases were only suspected, leaving uncertainties in diagnosis and clinical management.

The objective of this study was to further characterize this challenging subset of *SS18* FISH-negative/atypical SS using tools that have recently become available, including next-generation sequencing and two monoclonal antibodies that recognize SS18-SSX and the SSX carboxy-terminal (C-term) antigen. The latter reagents identify the most common SS18-SSX fusion breakpoint and the C-term portion of SSX, respectively. Previous large studies[16–18] collectively reported 87–95% sensitivity and 100% specificity for SS18-SSX antibody, and 92–100% sensitivity and 93–96% specificity for SSX (C-term) antibody. Our investigation led to the discovery of novel *SSX1* fusions to non-*SS18* genes in a small subset of SS.

MATERIALS AND METHODS
Cases
After approval by the institutional review board (Approval No. 2014-089), we retrieved cases that were diagnosed as SS, or as sarcoma most consistent with SS, from the pathology archive of the National Cancer Center Hospital (Tokyo, Japan) from January 2008 to March 2021. All cases were histologically reviewed with available reports by a bone/soft tissue pathologist (AY). After excluding several cases that were found to represent different diseases, the diagnoses of 158 SS cases were confirmed. The patients consisted of 83 males and 75 females, with a median age of 42.5 years (range, 5–87 years). The histological subtype was monophasic in 131 cases and biphasic in 27 cases, and a poorly differentiated pattern was recognized in 40 cases (37 in monophasic; three in biphasic). One or more ancillary tests were previously performed for all cases. Among all cases, 99 were previously subjected to *SS18* break-apart FISH assay. Of these, 88 cases were reported as positive (including seven cases with an isolated 5′ pattern), eight were negative, and three were indeterminate owing to atypical signal patterns. Atypical patterns include small isolated 3′ signals with equivocally (narrowly) split 5′/3′ (n = 2) and equivocally (narrowly) split 5′/3′ (n = 1). The FISH-negative/atypical cohort (n = 11, representing 11% of SS tested by FISH) formed the basis of this study. Among the 59 tumors that were not subjected to FISH assays, 12 tested positive for *SS18-SSX* fusion by RT-PCR and/or sequencing. The remaining 47 cases did not receive molecular testing, among which 36 were tested for SMARCB1 immunohistochemistry and all showed reduced SMARCB1 expression. The remaining 11 (recent) cases were diagnosed based on positive SS18-SSX immunohistochemical staining after the introduction of this recently developed antibody.

Immunohistochemistry
Immunohistochemistry was performed on whole tissue sections. The primary antibodies used were SS18-SSX (E9X9V, 1:2000, Cell Signaling Technology, Danvers, MA, USA) and SSX (C-term) (E5A2C, 1:2000, Cell Signaling Technology). Antigen retrieval was performed using Target Retrieval Solution pH 9 (Dako, Glostrup, Denmark) in water bath. The slides were incubated with the primary antibody for 1 h and subsequently labeled using the EnVision system (Dako). Other immunohistochemical results were retrieved from the pathology reports or were performed afresh when needed, using the following primary antibodies: cytokeratin (AE1/AE3, 1:100; Dako), EMA (E29, 1:100; Dako), TLE1 (M-101, 1:200; Santa Cruz Biotechnology, Dallas, TX, USA), BCOR (C-10, 1:200; Santa Cruz), CD34 (QBEnd10, 1:100; Dako), SMARCB1 (25/BAF47, 1:100; BD Biosciences, Franklin Lakes, NJ, USA), and MUC4 (8G7, 1:400; Santa Cruz).

FISH
SS18 FISH assay was previously performed using the *SS18* Split Dual Color FISH Probe (Abbott Molecular, Abbott Park, IL, USA). *EWSR1* Split Dual Color

FISH Probe (Abbott Molecular) and *MN1* Split Dual Color FISH Probe (Cytotest, Rockville, MD, USA) were used in this study when needed. FISH images were captured using the Metafer Slide Scanning Platform (Metasystem, Altlussheim, Germany) and at least 60 non-overlapping tumor cells were evaluated. Tumors in which >20% of the tumor cells showed split 5′/3′ or isolated 5′ signals were considered positive for rearrangement.

Sequencing
Total RNA was extracted from 4 μm-thick FFPE tumor sections using an RNeasy FFPE kit (Qiagen, Hilden, Germany). An RNA sequencing library was prepared using a TruSight RNA Pan-Cancer library kit (Illumina, San Diego, CA, USA). The library was subjected to paired-end sequencing on a MiSeq DNA sequencer (Illumina, cases 1, 2, 3, 4, 6, and 7) or NextSeq sequencer (Illumina, cases 5 and 9). For case 1, the paired-end reads were aligned to known RNA sequences in the RefSeq, Ensembl, and LincRNA databases using the BWA-MEM program. For cases 2, 3, 4, 6, and 7, fusion genes were identified using the RNA-Seq Alignment application (Illumina). For cases 5 and 9, fusion genes were searched using the FusionCatcher ver 1.00 algorithm. Novel and/or rare fusions (*EWSR1-SSX1*, *MN1-SSX1*, and *SS18L1-SSX1*) were confirmed using RT-PCR and Sanger sequencing with the primers listed in Supplementary Table 1.

DNA methylation-based classification
Adequate materials were available for methylation analysis for case 1 (*EWSR1-SSX1*), case 4 (*MN1-SSX1*), and case 5 (*SS18L1-SSX1*). One SS with *SS18-SSX1* was also analyzed as a positive control. Genomic DNA was extracted from FFPE sections using a DNeasy Blood & Tissue Kit (Qiagen). Bisulfite modification was performed using 500 ng genomic DNA and an EZ DNA Methylation Kit (Zymo Research Corporation, Irvine, CA, USA). The bisulfite-modified DNA was retrieved using an Infinium HD Assay Kit FFPE Restore Kit (Illumina). The samples were subjected to methylation analysis using Infinium MethylationEPIC BeadChips (EPIC, Illumina).

The methylation profiling classifier developed by the German Cancer Research Center (DKFZ) was used (DKFZ classifier, https://www.molecular neuropathology.org/msp/) to assign subtype scores for each tumor. All computational analyses were performed in R version 4.0.4. Raw signal intensities were obtained from IDAT files of 4 SS samples using the minfi Bioconductor package version 1.34.0. Unprocessed IDAT files from 1077 samples were downloaded from the NCBI Gene Expression Omnibus (GEO) under accession number GSE140686 and used as a reference[19]. Datasets of 1081 Illumina EPIC and 450k samples were merged using the combineArrays function in minfi. A correction for the type of material tissue (FFPE/frozen) and array (450k/EPIC) was performed with the removeBatchEffect function in the limma package (version 3.44.3). The methylated and unmethylated signals were individually corrected and the beta values were calculated using an offset of 100. After probe-filtering criteria were applied according to the GitHub repository (https://github.com/mwsill/mnp_training), 428,230 probes were retained for subsequent analysis.

To perform unsupervised non-linear dimension reduction, the 10,000 most variable probes (according to standard deviation) were selected among 1077 reference samples. The *t*-distributed stochastic neighbor embedding (*t*-SNE)[20] plots for the 4 SS and 1077 reference samples were made using the Rtsne package (version 0.15) using 3000 iterations and a perplexity value of 30.

RNA differential expression analysis
Total RNA was extracted from 10 μm FFPE sections using the RNeasy FFPE kit (Qiagen). RNA quality was assessed using DV200 values, and cases with DV200 more than 30% were included for library preparation. An input of 75 ng of total FFPE RNA was used with the TruSeq RNA Access Library Prep Kit, which captures the coding transcriptome/RNA exome (Illumina). Libraries were quantified by real-time PCR using KAPA Library Quantification kits (Kapa Biosystems, Wilmington, MA, USA) on ABI StepOne thermocycler, and sequenced on a Miseq (Illumina) using a 76 cycle, paired-end protocol providing approximately 10–12 million reads per sample. All RNA-seq reads were aligned to the human reference genome (GRCh19) using RNA-Seq Alignment (version 2.0.2) and RNA-Seq Differential Expression (version 1.0.1) (Illumina).

RESULTS
Summary of SS18 FISH-negative/atypical synovial sarcoma
The results are summarized in Table 1. Briefly, 11 *SS18* FISH-negative/atypical synovial sarcomas occurred in three men and

Table 1. Summary of synovial sarcoma cases with negative/atypical *SS18* FISH patterns.

Case	Age/Sex	Histology	*SS18* FISH	SMARCB1 IHC	SS18-SSX IHC	SSX (C-term) IHC	RNA-seq
1	45/Female	Monophasic (por)	Neg	Intact	Neg	Pos	*EWSR1*(e10)-*SSX1*(e4)
2	63/Female	Biphasic	Neg	Intact	Neg	Pos	*EWSR1*(e10)-*SSX1*(e5)
3	53/Male	Monophasic (por)	Neg	Intact	Neg	Pos	*EWSR1*(e10)-*SSX1*(e5)
4	47/Female	Monophasic	Neg	Intact	Neg	Pos	*MN1*(e1)-*SSX1*(e5)
5	26/Female	Monophasic	Neg	Reduced	Pos (weak)	Pos	*SS18L1*(e10)-*SSX1*(e6)
6	63/Female	Monophasic	Neg	Reduced	Pos	NA	*SS18*(e10)-*SSX2*(e6)
7	5/Male	Monophasic	Neg	Reduced	Pos	NA	*SS18*(e10)-*SSX2*(e6)
8	45/Male	Biphasic	Neg	Reduced	Pos	NA	NA
9	23/Female	Monophasic (por)	Atypical	Intact	Pos	NA	*SS18*(e10)-*SSX2*(e6)
10	71/Female	Monophasic	Atypical	Reduced	Pos	NA	NA
11	56/Female	Monophasic	Atypical	Reduced	Pos	NA	NA

NA not available, *por* poorly differentiated pattern, *Pos* positive, *Neg* negative, *IHC* immunohistochemistry, *FISH* fluorescence in situ hybridization.

eight women with a median age of 47 years (range, 5–71 years). Six cases were primary to the somatic soft tissue, while five arose in the internal trunk. Nine cases were monophasic and two were biphasic, with three cases at least focally showing a poorly differentiated pattern. AE1/AE3 and/or EMA was expressed, at least focally, in all ten tumors that were tested. TLE1 was expressed in all seven tumors tested. SMARCB1 expression was reduced in 6 of 11 tumors. The *SS18* FISH pattern was negative in eight tumors and atypical/uninterpretable in three tumors. All 11 tumors were tested using SS18-SSX immunohistochemistry, and SSX (C-term) staining was performed in five tumors. Eight tumors were successfully analyzed by targeted RNA sequencing.

Recurrent EWSR1-SSX1 fusions in synovial sarcomas

Cases 1–3 were immunohistochemically negative for SS18-SSX and diffusely positive for SSX (C-term), while SMARCB1 expression was not reduced. RNA sequencing showed that case 1 harbored an in-frame *EWSR1* (exon 10, NM_001163285.2)-*SSX1* (exon 4, NM_005635.4) fusion, and cases 2 and 3 harbored identical in-frame *EWSR1* (exon 10, NM_001163285.2)-*SSX1* (exon 5, NM_005635.4) fusions. The *EWSR1-SSX1* fusions were confirmed using RT-PCR, Sanger sequencing, and *EWSR1* break-apart FISH assays in all three cases. Their clinicopathological data are provided below and are summarized in Tables 1 and 2. The pathological findings are illustrated in Figs. 1 and 2.

Case 1 was a 45-year-old woman who presented with a 5 cm intramuscular mass in the right thigh. After neoadjuvant chemotherapy, the patient received wide en bloc tumor resection and adjuvant chemotherapy. The tumor locally recurred three times as 1.5–3.5 cm masses over 8 years. Each recurrence was surgically resected and treated with chemotherapy. The tumor ultimately recurred in the inguinal and paraaortic lymph nodes, and pleura, and the patient is alive with disease 10.5 years after the initial surgery. The examined specimen was a resection of the third local recurrence, in which the tumor showed intersecting dense fascicles and whorls of spindle cells with a mitotic count of 15/10 high power fields (HPF; 0.237 mm^2). No necrosis was observed. A poorly differentiated round cell pattern (30%), which was focally associated with sclerosis, and myxoid change (<5%) were also observed.

Case 2 involved a 63-year-old woman who presented with dyspnea and cough. A workup identified a 7 cm focally calcified mass in the left lung and mediastinum, pleural dissemination, and pleural fluid. The tumor was partially excised, and the patient is alive on chemotherapy 4 months after presentation. The tumor displayed a biphasic histology consisting of papillary to glandular epithelial structure and intervening fascicles of spindle cell proliferation. The tumor cells were monomorphic with mitotic

activity (5/10 HPF). Necrosis and focal metaplastic ossification were present.

Case 3 was a 53-year-old man who had a 5 cm heart mass with pericardial fluid that was identified in a health check-up. The tumor was resected with an initial diagnosis elsewhere of probable benign spindle cell tumor. The tumor locally recurred in 2 years and was excised again. The patient is alive with disease 2.5 years after the initial presentation. The recurrent tumor showed poorly differentiated monophasic histology consisting of fascicular proliferation of monomorphic spindle cells with focal whirling and necrosis. Mitosis was brisk (>20/10 HPF).

Discovery of an MN1-SSX1 fusion

Case 4 showed negative SS18-SSX protein expression, diffuse SSX (C-term) positivity, and intact SMARCB1 expression. RNA sequencing identified an in-frame *MN1* (exon 1, NM_002430.3)-*SSX1* (exon 5, NM_005635.4) fusion. The presence of the fusion was confirmed using RT-PCR and Sanger sequencing. *MN1* break-apart FISH assay did not identify a positive pattern of *MN1* rearrangements, despite the sequencing results.

The patient was a 47-year-old woman who presented with a 15-cm mass in the retroperitoneum. The tumor was resected with a segment of inferior vena cava. Multiple lung metastases were identified subsequently, several of which were resected. The patient is currently alive with additional small lung metastases at 14 months after initial surgery. The tumor showed alternating loose and dense areas. The latter areas were composed of intersecting and swirling fascicles of uniform spindle cells with a mitotic count of 3/10 HPF. Nuclear palisading was occasionally prominent. The loose areas displayed myxoid stroma with mast cells. Other findings include hemangiopericytomatous vessels and wiry collagen associated with scattered calcification. No necrosis or poorly differentiated component was observed. The metastatic tumors in the lung showed similar histology to the primary. Additional clinicopathological data are provided in Tables 1 and 2, and the pathological findings are illustrated in Fig. 3.

Identification of an SS18L1-SSX1 fusion

Case 5 was weakly positive for SS18-SSX protein and strongly positive for SSX C-term. SMARCB1 expression was reduced. RNA sequencing identified an in-frame *SS18L1* (exon 10, NM_198935.3)-*SSX1* (exon 6, NM_005635.4) fusion, which was confirmed using RT-PCR and Sanger sequencing.

The patient was a 26-year-old woman with a 7.1 cm intramuscular mass in the right thigh. After neoadjuvant chemotherapy, the patient received wide en bloc tumor resection with negative margins and adjuvant treatment. The patient is alive with no evidence of disease 8.5 years after the surgery. The resected tumor

Table 2. Additional clinicopathological findings of synovial sarcoma cases with novel and/or rare *SSX1* fusions.

Case	Fusion genes	Tumor site	Size (cm)	Positive (retained) IHC	Negative IHC	Treatment	Outcome
1	EWSR1-SSX1	Thigh	5	Bcl2, BCOR(f), CK(f), EMA, TLE1	CCNB3, CD34, CD99, desmin, MUC4, NKX2.2, S100, SMA	Surgery, Chemo	Local recurrence × 3, metastases to LN and pleura, AWD (10.5 y)
2	EWSR1-SSX1	Mediastinum	7	Bcl2, BCOR(f), CK, H3K27me3, TLE1	Calretinin, myogenin, TTF1	Surgery, Chemo	AWD (4 mos)
3	EWSR1-SSX1	Heart	5	Bcl2, CD99, EMA, H3K27me3, TLE1	BCOR, CD34, CK, desmin, ERG, myogenin, S100, SMA, STAT6	Surgery	Local recurrence, AWD (2.5 y)
4	MN1-SSX1	Retroperitoneum	15	BCOR, CK(f), EMA, H3K27me3, PanTRK(f), TLE1	CCNB3, CD34, CD99, desmin, DOG1, ER, h-caldesmon, MUC4, myogenin, NKX2.2, S100, SATB2, SMA, SOX10, STAT6	Surgery	Metastases to lung, AWD (14 mos)
5	SS18L1-SSX1	Thigh	7.1	Bcl2(f), CD99(f), CK(f), EMA, TLE1	BCOR, CD34, desmin, myogenin, S100, SMA	Surgery, Chemo	NED (8.5 y)

IHC immunohistochemistry, *CK* cytokeratin, *EMA* epithelial membrane antigen, *SMA* smooth muscle actin, *f* focal expression, *Chemo* chemotherapy, *AWD* alive with disease, *NED* no evidence of disease, *LN* lymph nodes.

showed intersecting dense fascicles of spindle cells with a mitotic count of 2/10 HPF. Myxoid change (10%) and calcification/ossification (<5%) were present, but a poorly differentiated component was not observed. The tumor was within the skeletal muscle, and there was no clinical and histological evidence of intraneural tumor location despite extensive sampling (15 tumor sections). Additional clinicopathological data are provided in Tables 1 and 2. The pathological findings are illustrated in Fig. 4.

SS18-SSX2 fusions in synovial sarcoma with negative/atypical SS18 FISH

The remaining six cases (cases 6–11) showed strong diffuse SS18-SSX expression. RNA sequencing was successfully performed in cases 6, 7, and 9, and canonical *SS18* (exon 10, NM_001007559.3)-*SSX2* (exon 6, NM_003147.5) fusion transcripts were identified. Additional clinicopathological data are provided in Table 1 and the pathological findings are illustrated in Fig. 5. The atypical FISH patterns observed in cases 9–11 are shown in Supplementary Fig. 1.

DNA methylation-based classification

The tumor in case 5 (*SS18L1-SSX1*) and one control tumor with canonical *SS18-SSX1*, matched with "methylation class synovial sarcoma" by the DKFZ classifier (score = 0.99). The two remaining samples (case 1 with *EWSR1-SSX1* and case 4 with *MN1-SSX1*) showed no matching methylation classes (calibrated score ≥0.3). However, t-SNE analysis showed that both cases 1 (*EWSR1-SSX1*) and 5 (*SS18L1-SSX1*), along with a control *SS18-SSX1*-positive tumor, clustered within the SS cluster. The remaining 1 sample (case 4 with *MN1-SSX1*) was located in the vicinity of, but not within, the Ewing sarcoma cluster (Fig. 6).

RNA differential expression analysis

As case 4 (*MN1-SSX1*) was not co-clustered with other synovial sarcomas by DNA methylation profiling, we attempted to probe for distinct mRNA expression patterns for this case. When case 4 (*MN1-SSX1*) was compared with a group of cases 2, 3, 6, and 7 (tumors with *EWSR1-SSX1* and *SS18-SSX2*), approximately 200 significantly upregulated or downregulated genes were identified with an adjusted p-value <0.05. However, the gene list did not include those that encode relevant immunohistochemical markers that are currently used in sarcoma diagnosis (Supplementary Table 2). We noted two genes, *KRT17* and *PRAME*, expression of which was upregulated and downregulated, respectively, in case 4. Their encoded proteins are occasionally assessed in diagnostic pathology; CK17 and PRAME immunostaining in case 4 was negative. In contrast, there was no significant expression difference in genes whose products can be used for SS diagnosis (*TLE1*, *BCL2*, *MUC1*, *KRT19*, *CD99*, and *BCOR*).

Validation of SS18-SSX immunohistochemistry

We validated the SS18-SSX immunohistochemistry sensitivity by staining 67 randomly selected SS samples that were not included in the above 11 tumors. All were previously tested positive for *SS18* FISH, *SS18-SSX* by RT-PCR/sequencing, and/or reduced SMARCB1 expression. The staining was positive for 66 tumors, with diffuse strong reactivity in 61 cases. These included a single case (25 years/male, chest wall, biphasic) with an *SS18-SSX4* fusion. Five tumors displayed weak to moderate intensity, all of which were positive for *SS18* FISH. The only tumor (38 years/male, abdominal wall, monophasic) that was negative for SS18-SSX staining was positive for *SS18* FISH. This tumor showed conventional histology and reduced SMARCB1 expression.

DISCUSSION

This study highlights an uncommon but recurrent challenge in the use of *SS18* FISH for SS diagnosis. We found that 11% of SS that were tested by *SS18* FISH assays produced negative or atypical/
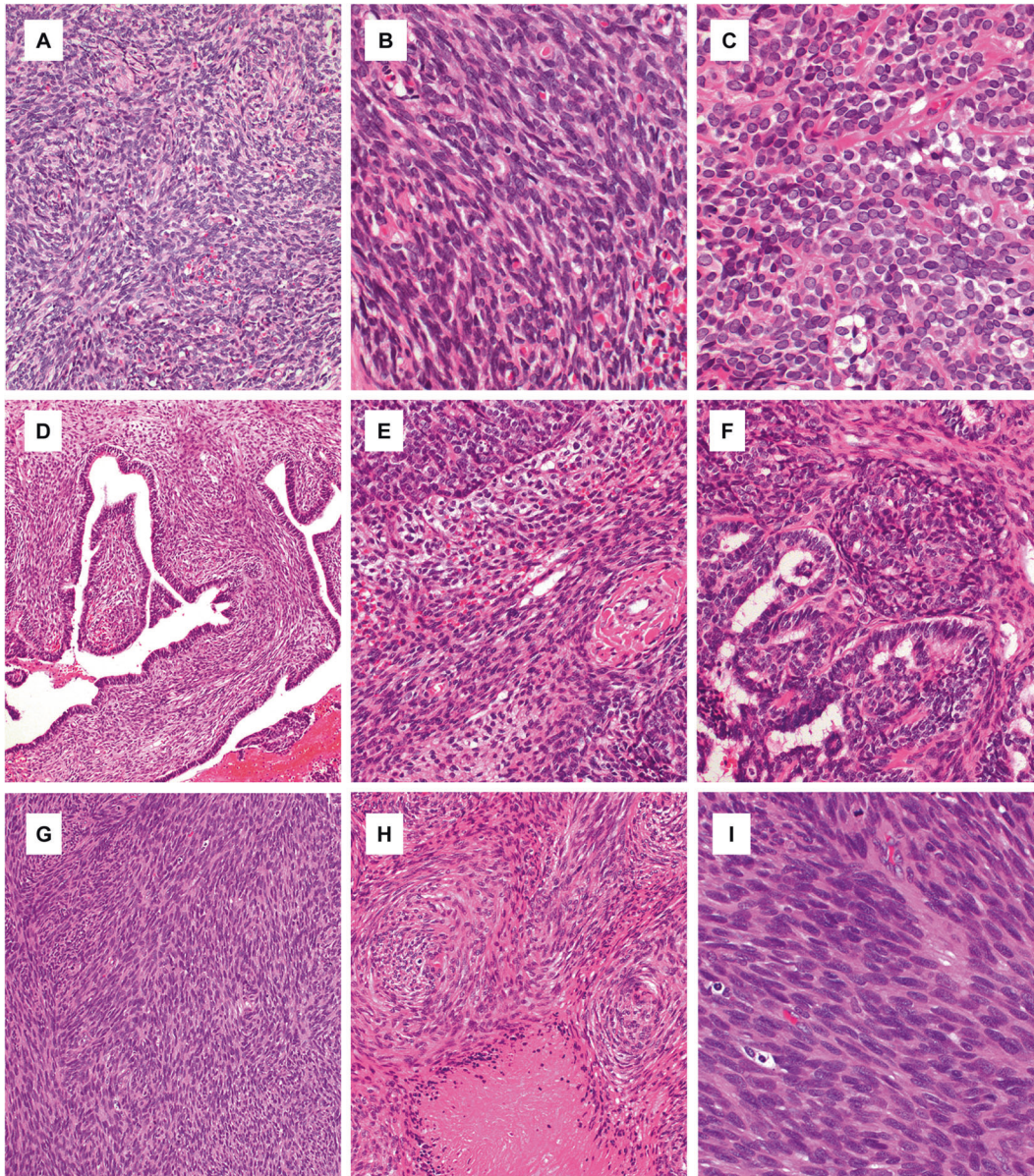
Fig. 1 Morphological findings of synovial sarcomas with *EWSR1-SSX1* fusions (cases 1–3). A–C Case 1 showed monophasic histology composed of swirling fascicles of uniform spindle cells (**A**, **B**). A poorly differentiated round cell component was focally present (**C**). **D–F** Case 2 showed papillary and glandular architecture (**D**). The tumor was biphasic, including fascicles of uniform spindle cells (**E**) and complex glandular formations of epithelial cells (**F**). **G–I** Case 3 displayed long fascicular (**G**) to whorled (**H**, necrosis is present in the bottom) spindle cell proliferation. The monomorphic tumor cells harbored a high nuclear/cytoplasmic ratio (**I**).

uninterpretable results, which was consistent with previous reports[9,10]. Because these events create problems in diagnostic practice, we performed an in-depth clinicopathological and molecular analysis of 11 such cases collected over a 13-year period, taking advantage of newly available RNA sequencing technology and monoclonal antibodies that recognize SS18-SSX and SSX (C-term).

The most remarkable finding of our study was the discovery of novel *SSX1* fusions in four cases: *EWSR1-SSX1* ($n = 3$) and *MN1-SSX1* ($n = 1$). These tumors occurred in the extremity ($n = 1$) and internal trunk ($n = 3$) in middle-aged adults. Histology of all four tumors fits well within the known spectrum of SS and comprised intersecting fascicles of uniform spindle cells with a high nuclear/cytoplasmic ratio. One tumor had a biphasic epithelial structure and two displayed a poorly differentiated pattern. Additional characteristics observed that are common in SS included an

alternating dense and loose pattern (cases 1, 2, and 4), swirling growth (cases 1, 3, and 4), hemangiopericytomatous vessels (case 4), scattered mast cells (cases 1 and 4), nuclear palisading (case 4), wiry collagen deposition (cases 2–4), and calcification/ossification (cases 2 and 4). The immunoprofiles were also typical, including frequent expression of CK, EMA, TLE1, and bcl-2, while CD34 expression was negative. As expected, SS18-SSX staining was negative and SSX (C-term) staining was diffusely positive, but SMARCB1 was not reduced. The incidence of these novel fusions in SS is estimated to be up to 2.5% (4/158), provided that all the SS cases in the initial cohort that did not receive *SS18* FISH showed *SS18-SSX* by sequencing, SS18-SSX immunoreactivity, and/or SMARCB1 reduction.

The histological classification of these cases was partly supported using a DNA methylation-based unsupervised clustering, in which the cases with *EWSR1-SSX1*, *SS18L1-SSX1*, and *SS18-SSX1* belonged to
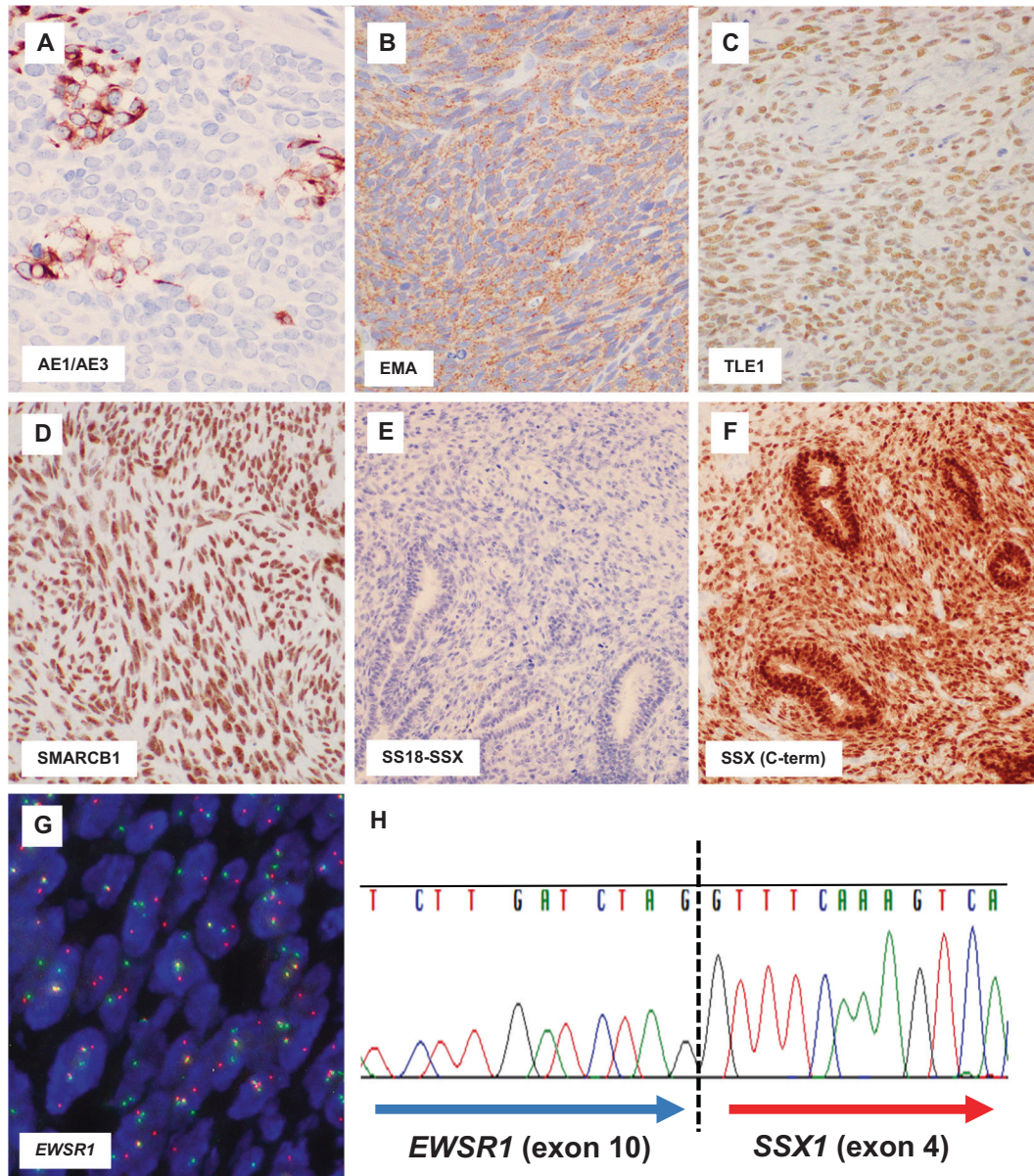
Fig. 2 **Immunohistochemical and molecular findings of synovial sarcomas with *EWSR1-SSX1* fusions (cases 1–3).** Two tumors each were variably positive for cytokeratin (**A** case 1) and EMA (**B** case 3). All were diffusely positive for TLE1 (**C** case 1). SMARCB1 immunoreactivity was not reduced (**D** case 3). SS18-SSX immunostaining was negative (**E** case 2), while SSX (C-term) immunostaining showed diffuse strong reactivity (**F** case 2, notice both epithelial and spindle cell components are positively stained in this biphasic tumor). Targeted RNA sequencing identified in-frame *EWSR1-SSX1* fusions in all three cases. The presence of the fusion genes was confirmed using *EWSR1* break-apart FISH assay (**G** case 3; split green and orange signals indicate gene rearrangements) and RT-PCR/Sanger sequencing (**H** case 1) for all three cases.

the known SS cluster. Interestingly, however, the case with the *MN1-SSX1* fusion was plotted away from the SS group, and in the vicinity of, albeit not within, the Ewing sarcoma cluster. This was a perplexing finding as the tumor showed a classic SS histology and immunoprofile without any round cells, and the Ewing sarcoma markers CD99 and NKX2.2[21] were entirely negative. Subsequent RNA differential expression analysis showed no significant expression differences in genes, whose encoded proteins are immunohistochemically assessed widely in the contemporary sarcoma diagnosis. DNA methylation-based sarcoma classification is an emerging research tool that has a high concordance with histological diagnosis, but is associated with occasional misleading or failed prediction[22]. Whether an *MN1-SSX1* sarcoma belongs to SS, as supported by its phenotype, or might represent an altogether new disease, requires future studies with a larger number of cases.

Although all three cases of SS with *EWSR1-SSX1* in this cohort showed fascicular spindle cell proliferation, a poorly differentiated round cell pattern, such as that focally observed in case 1, could mimic Ewing sarcoma when this pattern predominates in a sample. This represents a potential diagnostic pitfall if a panel-FISH approach with *EWSR1* and *SS18* break-apart probes is used. Careful phenotypic characterization including markers such as NKX2.2 and SSX (C-term) would be helpful in diagnosing difficult cases.

EWSR1 (22q12.2) encodes an RNA-binding protein that is a member of the FET family along with *FUS* and *TAF15*. EWSR1 protein possesses an N-terminal transcriptional activation domain and a C-terminal RNA-binding domain. In oncology, *EWSR1* is best known for its fusion with a number of 3′ partner genes, such as *EWSR1-FLI1* in Ewing sarcoma. As with other fusion events, the
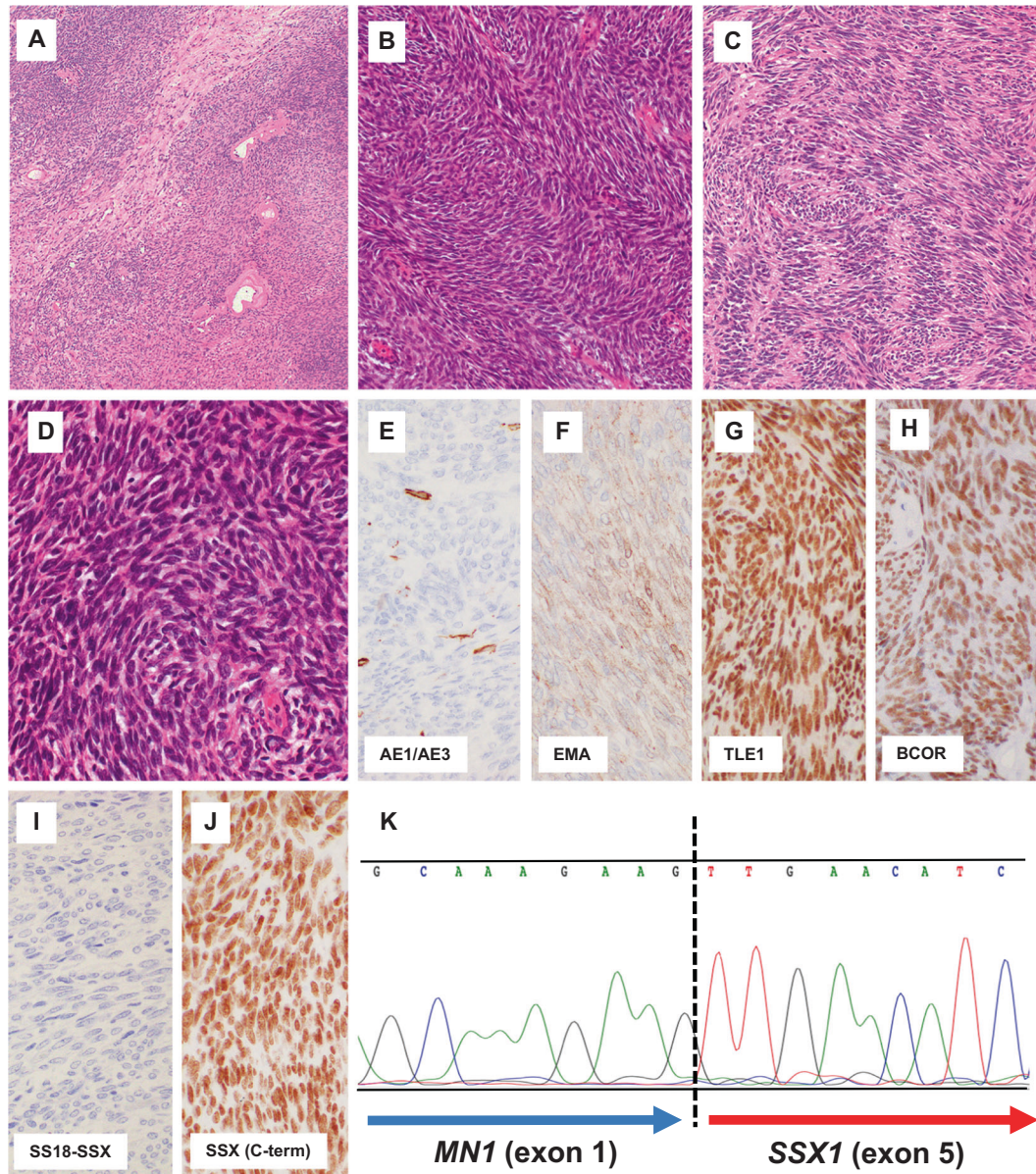
Fig. 3 Histological and molecular findings of synovial sarcoma with an *MN1-SSX1* fusion (case 4). The tumor showed alternating loose and dense areas (**A**), the latter composed of intersecting and swirling fascicles of spindle cells (**B**). Nuclear palisading was occasionally observed (**C**). The tumor cells were monomorphic and possessed a high nuclear/cytoplasmic ratio (**D**). Immunohistochemically, the tumor showed focal strong cytokeratin expression (**E**), diffuse weak EMA expression (**F**), and diffuse strong TLE1 (**G**), and BCOR (**H**) expressions. SS18-SSX immunostaining was negative (**I**), while SSX (C-term) immunostaining showed diffuse strong reactivity (**J**). Targeted RNA sequencing identified in-frame *MN1-SSX1* fusion transcripts, which were confirmed using RT-PCR/Sanger sequencing (**K**).

putative EWSR1-SSX1 fusion protein retains the N-terminal transcriptional activation domain (Fig. 7). However, SSX1 does not have a DNA-binding domain, unlike many other EWSR1 fusion partners. *MN1* (22q12.1) encodes a transcriptional coactivator, with no homology to other proteins. The MN1 protein has an N-terminal nuclear localization signal, proline-rich sequences, and two polyglutamine stretches, but lacks a DNA-binding domain[23]. MN1 interacts with several transcription factors including PBX1, PKNOX1, and the E3 ubiquitin ligase RING1[24]. Although originally described as being disrupted in meningioma[23], the oncogenic role of *MN1* is best known in acute myeloid leukemia (AML), a rare subset of which harbors an *MN1-ETV6* fusion[25]. MN1 overexpression has also been associated with poor prognosis in AML with normal karyotype[26]. More recently, brain tumors with *MN1* alterations, most commonly *MN1-BEND2* fusions, were

identified to form a distinct DNA methylation class with variable histology (such as astroblastoma), immunophenotype, and clinical outcome[27,28]. *MN1* C-terminal truncating mutations define a distinct syndrome with craniofacial and brain abnormality[24,29].

The existence of SS with fusions that lack involvement of *SS18* or its paralog *SS18L1* sheds new light on SS pathogenesis. The mechanisms of action exerted by the SS18-SSX fusion oncoprotein include disruption of epigenetic control, mainly by disturbing the balance between the polycomb repressive complex (PRC) and the BAF chromatin remodeling complex. In one model, SS18-SSX recruits PRC2 by bridging its member TLE1 and activating transcriptional factor 2 (ATF2), thereby repressing ATF2 targets such as the tumor suppressor genes *CDKN2A* and *EGR1*[30]. More recent studies emphasize crucial roles of SS18-SSX-containing "hijacked" BAF complexes, which target and reactivate genes
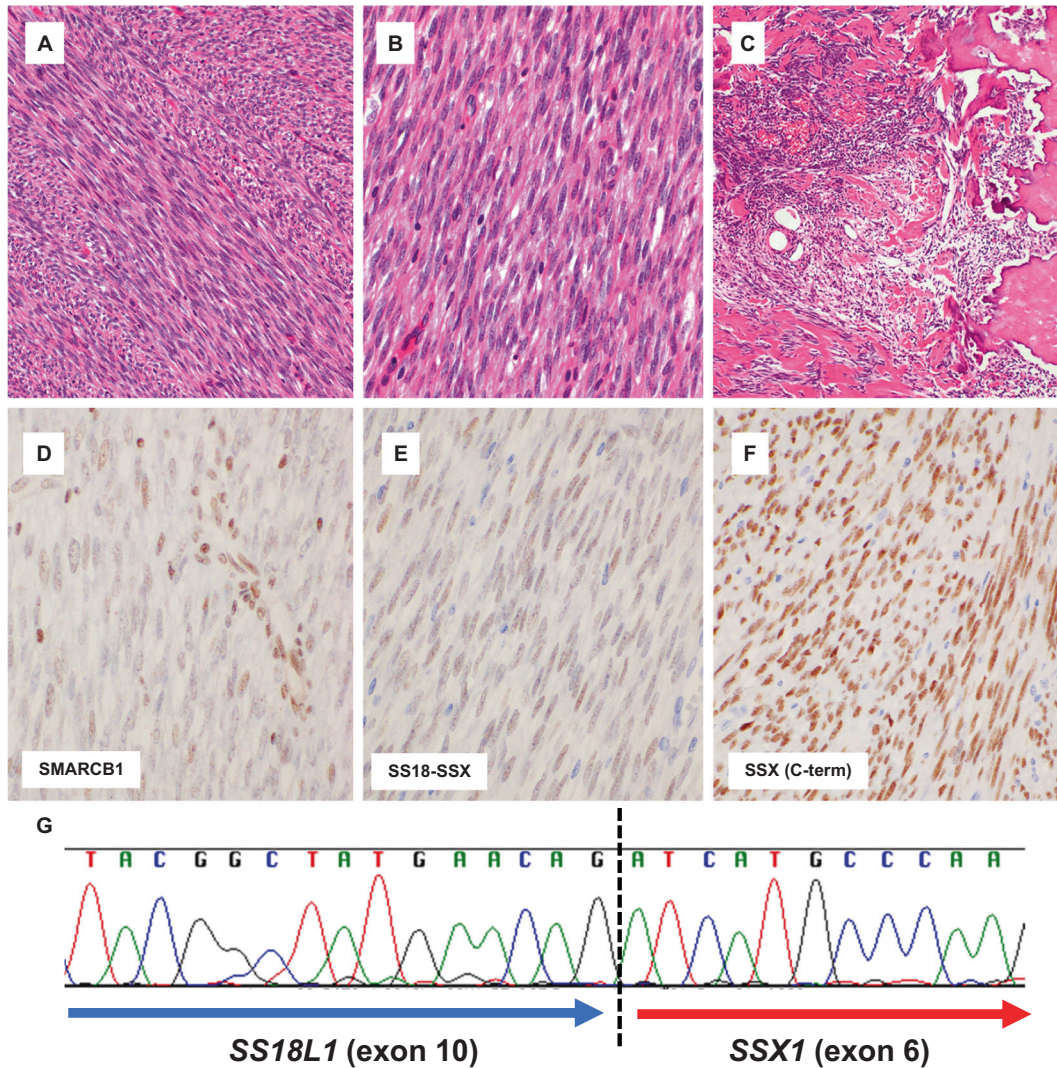
Fig. 4 **Histological and molecular findings of synovial sarcoma with an *SS18L1-SSX1* fusion (case 5).** The tumor consisted of fascicular proliferation of uniform spindle cells (**A**, **B**). Focal stromal calcification/ossification was observed (**C**). SMARCB1 immunoreactivity was reduced (**D** notice strongly stained endothelial cells and immune cells as internal positive controls). SS18-SSX immunostaining was weakly positive (**E** compare with the intensity observed in an *SS18-SSX2*-positive tumor, depicted in Fig. 5C), while SSX (C-term) immunostaining showed diffuse strong reactivity (**F**). Targeted RNA sequencing identified *SS18L1-SSX1* fusion transcripts, which were confirmed using RT-PCR/Sanger sequencing (**G**).
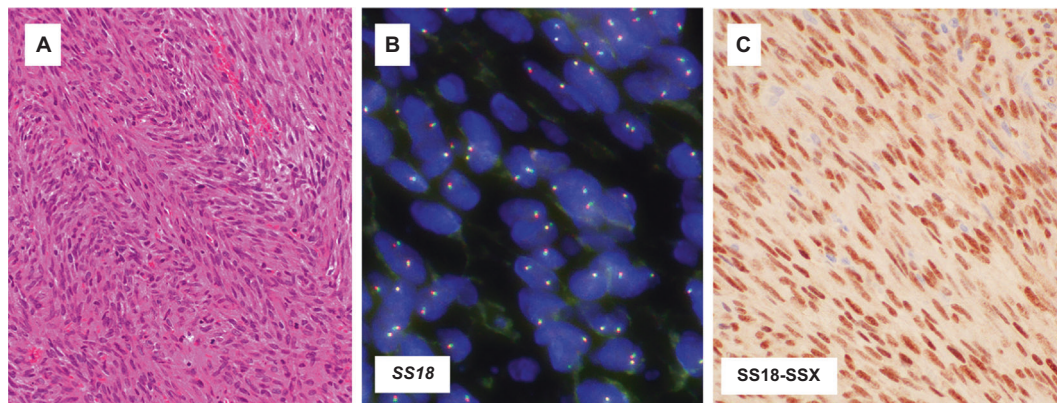

Fig. 5 ***SS18* FISH false-negative synovial sarcoma with an *SS18-SSX2* fusion (case 7).** The tumor showed classic monophasic synovial sarcoma histology (**A**). However, *SS18* FISH assay demonstrated no signals indicating gene rearrangement (**B** all tumor cell nuclei harbored 2 yellow or fused green/orange signals). SS18-SSX immunohistochemistry showed diffuse strong expression of the fusion oncoprotein (**C**). Targeted RNA sequencing identified an *SS18-SSX2* fusion.
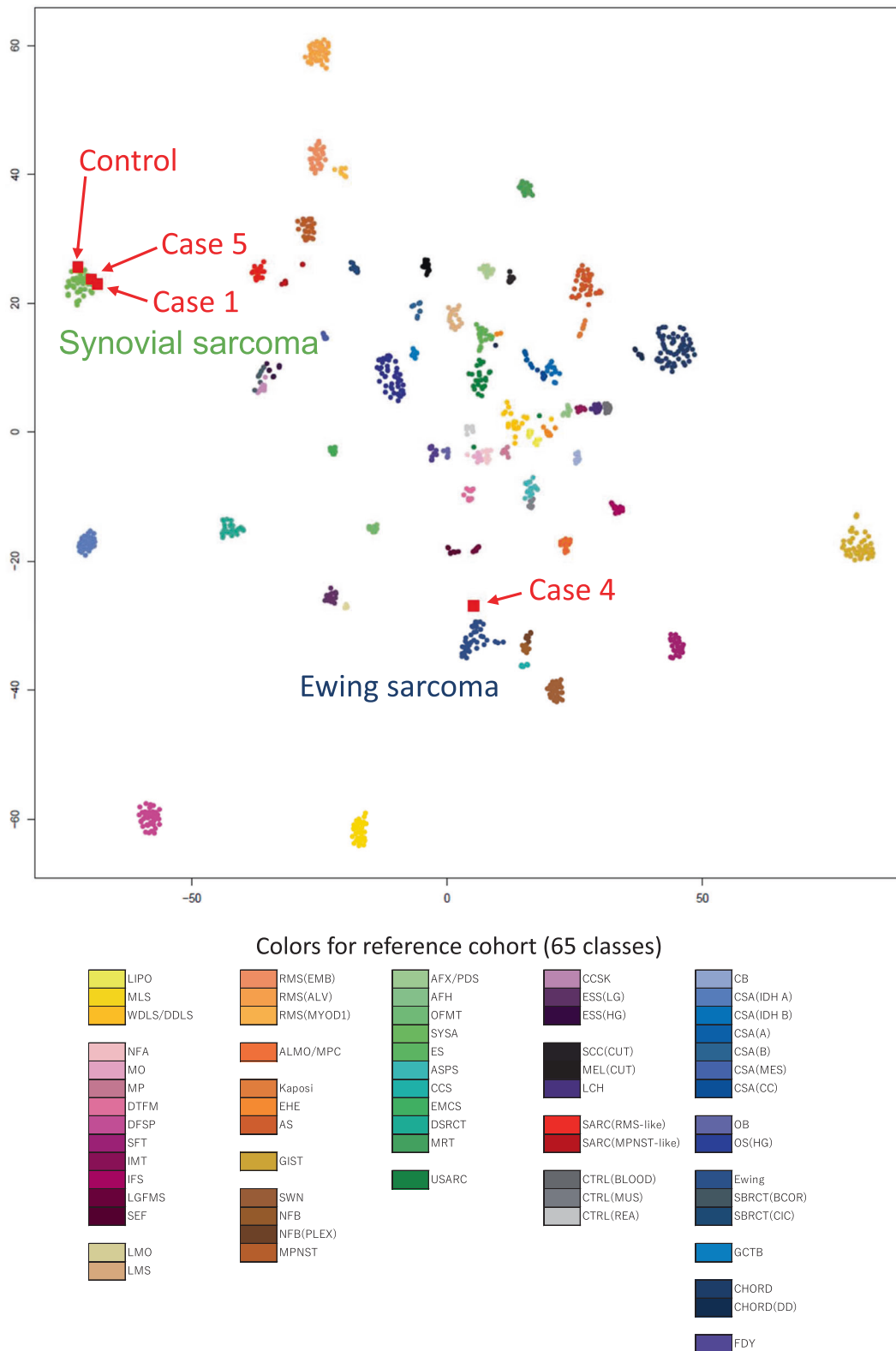
Fig. 6 DNA methylation-based unsupervised clustering. The reference cohort ($n = 1077$) and our synovial sarcoma samples ($n = 4$; one control with *SS18-SSX1*, case 1 with *EWSR1-SSX1*, case 4 with *MN1-SSX1*, and case 5 with *SS18L1-SSX1*) were plotted using *t*-distributed stochastic neighbor embedding (*t*-SNE) dimensionality reduction. Our synovial sarcomas are indicated as red squares. Tumor name abbreviations and the color code of the 62 reference tumors and three control DNA methylation classes were the same as in Koelsche et al.[19]. Cases 1 and 5 are plotted within the synovial sarcoma cluster along with a positive control, while case 4 is plotted in the vicinity of Ewing sarcoma.
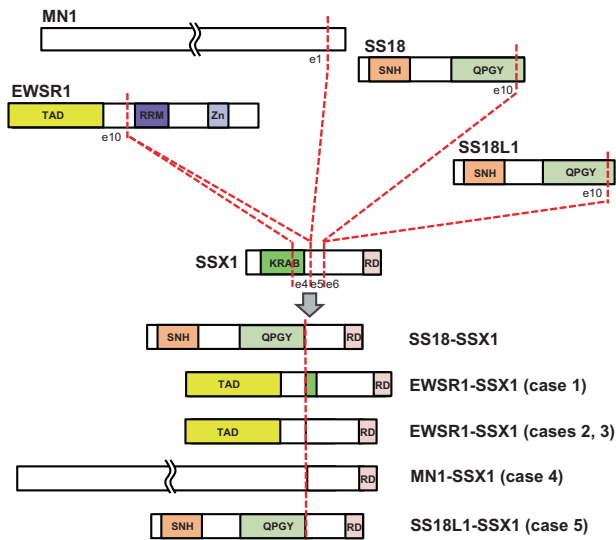
Fig. 7 Schematic predicted fusion protein structures of novel and/ or rare SSX1 fusions in cases 1–5 compared to the canonical SS18-SSX1. TAD transactivating domain, RRM RNA recognition motif, Zn Zinc finger motif, SNH SS18 N-terminal homology, QPGY glutamine/ proline/glycine/tyrosine-enriched domain, KRAB Krüppel-associated box domain, RD SSX repressor domain.

bivalently marked with H3K4me3 and H3K27me3[6]. These BAF complexes also interact with KDM2B, a member of PRC1.1, and bring together BAF and PRC1.1 on unmethylated CpG islands to aberrantly reactivate the expression of developmentally regulated genes[31]. Detailed functional studies are clearly needed to understand the role of *EWSR1-SSX1* and *MN1-SSX1* in SS. However, the recurrent presence of *EWSR1-SSX1* in three cases, shared 3′ *SSX1* to canonical fusions, and the abundant SSX (C-term) immunoreactivity in tumor nuclei suggest that these *SSX1* fusions play driver roles. Because neither EWSR1 nor MN1 is a component of the BAF complex, EWSR1-SSX and MN1-SSX1 fusion oncoproteins are not expected to be incorporated into the BAF complex in the same way as SS18-SSX. This hypothesis is partly supported by intact (not reduced) SMARCB1 immunoexpression in all four tumors harboring these new fusions.

However, it is conceivable that the downstream effect of these fusions may converge into the same molecular perturbation incurred by SS18-SSX. It is proposed that the EWSR1 fusion protein mediates liquid–liquid phase separation owing to the prion-like intrinsically disordered region (IDR) found in the EWSR1 N-terminal low-complexity sequence, which is conserved in the fusion product. EWSR1 fusion protein binds with BAF complex without altering the core protein composition likely in these condensates, thereby altering genome-wide transcription patterns[32,33]. In Ewing sarcoma, EWSR1-FLI1 recruits the BAF complex via the IDR to GGAA microsatellite repeat enhancers to activate tumor-specific target genes[32]. Similarly, a substantial portion of MN1 consists of an IDR[24], and MN1 has recently been shown, in an abstract paper[34], to interact with the BAF complex via the IDR in *MN1*-driven AML. The *EWSR1-SSX1* and *MN1-SSX1* fusions that we identified conserve IDRs, and thus, it is tempting to speculate that the abnormal pattern of BAF complex recruitment promoted by these fusions might overlap with that induced by SS18-SSX-containing BAF complex, resulting in a shared transcriptional program leading to SS[6,35].

In this connection, emerging data suggest an interchangeable role of *SS18*, *EWSR1*, and *MN1* in fusion-driven oncogenesis. Recent reports documented two soft tissue tumors with *SS18-POU5F1*

fusions with a myoepithelial phenotype[36,37], and one of these tumors was clustered, by RNA expression profiling, with myoepithelial tumors containing *EWSR1-POU5F1*[36]. Similarly, one case of astroblastoma harboring an *EWSR1-BEND2* fusion was reported[38], instead of the more common *MN1-BEND2* fusions[27,39], as was an *MN1-PATZ1*-positive pediatric intracranial sarcoma with expression and phenotypes resembling *EWSR1-PATZ1*-positive sarcoma[40].

Very recently, Antonescu et al. reported two unusual sarcomas with *EWSR1* (exon 7)-*SSX1* (exon 5) fusions[41]. These tumors, which affected the extremities of young adults, showed nests and cords of epithelioid cells in a sclerotic background and were diffusely immunoreactive to cytokeratin, EMA, TLE1, and BCOR, while focally positive for MUC4. These tumors seemed distinct from SS that we describe herein, as they entirely lacked a fascicular spindle cell component. Keratin expression pattern (focal vs. diffuse) and the *EWSR1* fusion breakpoint (exon 10 vs. exon 7) were also different. However, further study is required to determine the relationship, as our case 1 focally exhibited sclerosis in a poorly differentiated round cell component (Supplementary Fig. 2), although sclerosis in this specimen could be related to previous excision. We conducted MUC4 staining for cases 1 and 4, and found that case 1 exhibited weak focal expression, which is a known phenomenon in a subset of SS[42].

One tumor harbored a known *SS18L1-SSX1* fusion. This is the 3rd such case in literature with an identical *SS18L1* (exon 10) to *SSX1* (exon 6) combination to that reported previously[3,4]. The tumor occurred in the lower extremity in a young adult, similar to the two previous cases, but unlike them, it was not associated with a peripheral nerve. The tumor displayed a classic monophasic histology and immunoprofile. Notably, SS18-SSX immunohistochemistry was weakly positive, rather than a typical strong intensity. SS18L1 and SS18 are ~60% homologous[4,43], and eight of the nine last amino acids of SS18 (QQRPYGYDQ) and SS18L1 (QQRPYGYEQ) before the breakpoint are identical, with the remaining amino acid being similar (Asp vs. Glu), suggesting close antigenicity and cross-reactivity to the SS18-SSX antibody. This adds further value to the SS18-SSX antibody, and weak SS18-SSX immunoexpression along with negative *SS18* FISH may predict an *SS18L1-SSX1* fusion. Interestingly, SMARCB1 staining was reduced in this case, similar to the tumors with *SS18-SSX* fusions. The oncogenic mechanism of SS18L1-SSX1 remains unclear, but SS18L1 (also known as CREST) is a component of the BAF complex, and is physiologically involved in the neuron-specific BAF, where SS18L1 replaces SS18 and plays an important role in dendrite development[43,44]. SS18L1-SSX1 chimeric protein may enter the BAF complex and cause downstream effects similar to SS18-SSX, including BAF47 eviction.

Lastly, 6 of 11 cases tested showed evidence of canonical *SS18-SSX* fusions despite the negative/atypical FISH results. All six cases showed strongly positive staining for SS18-SSX. Three cases tested by RNA sequencing harbored *SS18-SSX2* fusions. All these cases showed classic histology, with five displaying reduced SMARCB1 expression. The reason these tumors demonstrated negative/ atypical FISH signals may be cryptic or complex rearrangement that escaped the resolution of FISH, as speculated for other sarcoma types[45].

In conclusion, we investigated a small subset of SS that was negative or atypical in the *SS18* FISH assay and discovered novel and rare *SSX1* fusions to non-*SS18* genes. The expanded genetic landscape of SS carries significant diagnostic implications and advances our understanding of the oncogenic mechanism. Our data also underscore the value of next-generation sequencing and recently developed antibodies to SS18-SSX and SSX (C-term) for SS diagnosis.

REFERENCES

1. Terry, J. et al. TLE1 as a diagnostic immunohistochemical marker for synovial sarcoma emerging from gene expression profiling studies. *Am. J. Surg. Pathol.* **31**, 240–246 (2007).
2. Pelmus, M. et al. Monophasic fibrous and poorly differentiated synovial sarcoma: immunohistochemical reassessment of 60 t(X;18)(SYT-SSX)-positive cases. *Am. J. Surg. Pathol.* **26**, 1434–1440 (2002).
3. Kao, Y. C. et al. BCOR upregulation in a poorly differentiated synovial sarcoma with SS18L1-SSX1 fusion-A pathologic and molecular pitfall. *Genes Chromosomes Cancer* **56**, 296–302 (2017).
4. Storlazzi, C. T. et al. A novel fusion gene, SS18L1/SSX1, in synovial sarcoma. *Genes Chromosomes Cancer* **37**, 195–200 (2003).
5. Argani, P. et al. Novel SS18-NEDD4 gene fusion in a primary renal synovial sarcoma. *Genes Chromosomes Cancer* **59**, 203–208 (2020).
6. McBride, M. J. et al. The SS18-SSX fusion oncoprotein hijacks BAF complex targeting and function to drive synovial sarcoma. *Cancer Cell* **33**, 1128–1141 e1127 (2018).
7. Arnold, M. A. et al. A unique pattern of INI1 immunohistochemistry distinguishes synovial sarcoma from its histologic mimics. *Hum. Pathol.* **44**, 881–887 (2013).
8. Ito, J., Asano, N., Kawai, A. & Yoshida, A. The diagnostic utility of reduced immunohistochemical expression of SMARCB1 in synovial sarcomas: a validation study. *Hum. Pathol.* **47**, 32–37 (2016).
9. Amary, M. F. et al. Detection of SS18-SSX fusion transcripts in formalin-fixed paraffin-embedded neoplasms: analysis of conventional RT-PCR, qRT-PCR and dual color FISH as diagnostic tools for synovial sarcoma. *Mod. Pathol.* **20**, 482–496 (2007).
10. Chuang, H. C. et al. Reappraisal of TLE-1 immunohistochemical staining and molecular detection of SS18-SSX fusion transcripts for synovial sarcoma. *Pathol. Int.* **63**, 573–580 (2013).
11. Sun, B. et al. The diagnostic value of SYT-SSX detected by reverse transcriptase-polymerase chain reaction (RT-PCR) and fluorescence in situ hybridization (FISH) for synovial sarcoma: a review and prospective study of 255 cases. *Cancer Sci.* **99**, 1355–1361 (2008).
12. Ten Heuvel, S. E., Hoekstra, H. J. & Suurmeijer, A. J. Diagnostic accuracy of FISH and RT-PCR in 50 routinely processed synovial sarcomas. *Appl. Immunohistochem. Mol. Morphol.* **16**, 246–250 (2008).
13. Terry, J. et al. Fluorescence in situ hybridization for the detection of t(X;18)(p11.2;q11.2) in a synovial sarcoma tissue microarray using a breakapart-style probe. *Diagn. Mol. Pathol.* **14**, 77–82 (2005).
14. Guillou, L. et al. Detection of the synovial sarcoma translocation t(X;18) (SYT;SSX) in paraffin-embedded tissues using reverse transcriptase-polymerase chain reaction: a reliable and powerful diagnostic tool for pathologists. A molecular analysis of 221 mesenchymal tumors fixed in different fixatives. *Hum. Pathol.* **32**, 105–112 (2001).
15. Jiang, D. et al. Synovial sarcoma showing loss of a green signal in SS18 fluorescence in situ hybridization: a clinicopathological and molecular study of 12 cases. *Virchows Arch.* **471**, 799–807 (2017).
16. Baranov, E. et al. A novel SS18-SSX fusion-specific antibody for the diagnosis of synovial sarcoma. *Am. J. Surg. Pathol.* **44**, 922–933 (2020).
17. Perret, R., Velasco, V., Le Guellec, S., Coindre, J. M. & Le Loarer, F. The SS18-SSX antibody has perfect specificity for the SS18-SSX fusion protein: a validation study of 609 neoplasms including 2 unclassified tumors with SS18-Non-SSX fusions. *Am. J. Surg. Pathol.* **45**, 582–584 (2021).
18. Zaborowski, M. et al. When used together SS18-SSX fusion-specific and SSX C-terminus immunohistochemistry are highly specific and sensitive for the diagnosis of synovial sarcoma and can replace FISH or molecular testing in most cases. *Histopathology* **77**, 588–600 (2020).
19. Koelsche, C. et al. Sarcoma classification by DNA methylation profiling. *Nat. Commun.* **12**, 498 (2021).
20. van der Maaten, L. & Hinton, G. Visualizing data using t-SNE. *J. Mach. Learn. Res.* **9**, 2579–2605 (2008).
21. Yoshida, A. et al. NKX2.2 is a useful immunohistochemical marker for Ewing sarcoma. *Am. J. Surg. Pathol.* **36**, 993–999 (2012).
22. Lyskjaer, I. et al. DNA methylation-based profiling of bone and soft tissue tumours: a validation study of the 'DKFZ Sarcoma Classifier'. *J. Pathol. Clin. Res.* https://doi.org/10.1002/cjp2.215 (2021).
23. Lekanne Deprez, R. H. et al. Cloning and characterization of MN1, a gene from chromosome 22q11, which is disrupted by a balanced translocation in a meningioma. *Oncogene* **10**, 1521–1528 (1995).
24. Miyake, N. et al. Gain-of-function MN1 truncation variants cause a recognizable syndrome with craniofacial and brain abnormalities. *Am. J. Hum. Genet.* **106**, 13–25 (2020).
25. Buijs, A. et al. Translocation (12;22) (p13;q11) in myeloproliferative disorders results in fusion of the ETS-like TEL gene on 12p13 to the MN1 gene on 22q11. *Oncogene* **10**, 1511–1519 (1995).
26. Heuser, M. et al. High meningioma 1 (MN1) expression as a predictor for poor outcome in acute myeloid leukemia with normal cytogenetics. *Blood* **108**, 3898–3905 (2006).
27. Sturm, D. et al. New brain tumor entities emerge from molecular classification of CNS-PNETs. *Cell* **164**, 1060–1072 (2016).
28. Tauziede-Espariat, A. et al. Pediatric methylation class HGNET-MN1: unresolved issues with terminology and grading. *Acta Neuropathol. Commun.* **7**, 176 (2019).
29. Mak, C. C. Y. et al. MN1 C-terminal truncation syndrome is a novel neurodevelopmental and craniofacial disorder with partial rhombencephalosynapsis. *Brain* **143**, 55–68 (2020).
30. Su, L. et al. Deconstruction of the SS18-SSX fusion oncoprotein complex: insights into disease etiology and therapeutics. *Cancer Cell* **21**, 333–347 (2012).
31. Banito, A. et al. The SS18-SSX oncoprotein hijacks KDM2B-PRC1.1 to drive synovial sarcoma. *Cancer Cell* **33**, 527–541 e528 (2018).
32. Boulay, G. et al. Cancer-specific retargeting of BAF complexes by a prion-like domain. *Cell* **171**, 163–178 e119 (2017).
33. Linden, M. et al. FET family fusion oncoproteins target the SWI/SNF chromatin remodeling complex. *EMBO Rep.* **20**, e45766 (2019).
34. Riedel, S. S. et al. SWI/SNF dysregulation through a prion-like domain causes AML. *Blood* **134**, 2512 (2019).
35. Nacev, B. A. et al. The epigenomics of sarcoma. *Nat. Rev. Cancer* **20**, 608–623 (2020).
36. Antonescu, C. R., Agaram, N. P., Sung, Y. S., Zhang, L. & Dickson, B. C. Undifferentiated round cell sarcomas with novel SS18-POU5F1 fusions. *Genes Chromosomes Cancer* **59**, 620–626 (2020).
37. Shenoy, A. et al. Malignant round cell tumor with SS18-POU5F1 fusion: is it a myoepithelial neoplasm, a synovial sarcoma or a new entity? *Histopathology* **77**, 681–684 (2020).
38. Yamasaki, K. et al. Spinal cord astroblastoma with an EWSR1-BEND2 fusion classified as a high-grade neuroepithelial tumour with MN1 alteration. *Neuropathol. Appl. Neurobiol.* **46**, 190–193 (2020).
39. Hirose, T. et al. Astroblastoma: a distinct tumor entity characterized by alterations of the X chromosome and MN1 rearrangement. *Brain Pathol.* **28**, 684–694 (2018).
40. Burel-Vandenbos, F. et al. A polyphenotypic malignant paediatric brain tumour presenting a MN1-PATZ1 fusion, no epigenetic similarities with CNS high-grade neuroepithelial tumour with MN1 alteration (CNS HGNET-MN1) and related to PATZ1-fused sarcomas. *Neuropathol. Appl. Neurobiol.* **46**, 506–509 (2020).
41. Antonescu, C. R. et al. Sarcomas with sclerotic epithelioid phenotype harboring novel EWSR1-SSX1 fusions. *Genes Chromosomes Cancer* https://doi.org/10.1002/gcc.22970 (2021 Epub).
42. Doyle, L. A. et al. MUC4 is a highly sensitive and specific marker for low-grade fibromyxoid sarcoma. *Am. J. Surg. Pathol.* **35**, 733–741 (2011).
43. Aizawa, H. et al. Dendrite development regulated by CREST, a calcium-regulated transcriptional activator. *Science* **303**, 197–202 (2004).
44. Staahl, B. T. et al. Kinetic analysis of npBAF to nBAF switching reveals exchange of SS18 with CREST and integration with neural developmental pathways. *J. Neurosci.* **33**, 10348–10361 (2013).
45. Yoshida, A. et al. CIC break-apart fluorescence in-situ hybridization misses a subset of CIC-DUX4 sarcomas: a clinicopathological and molecular study. *Histopathology* **71**, 461–469 (2017).

AUTHOR CONTRIBUTIONS
A.Y. designed the project, performed pathology review, and conducted IHC and FISH analyses. Y.A., T.K., E.R., N.H., T.S., H.I. and T.M. performed sequencing. K.Sa., Y.M. and K.I. performed DNA methylation analysis. K.Su., M.K., and Y.Y. and A.K. provided samples and clinical data. A.Y. wrote the original draft, which was reviewed and approved by all authors.

COMPETING INTERESTS
The authors declare no competing interests.

ETHICS APPROVAL

The study was approved by the institutional review board at the National Cancer Center Hospital, Tokyo, Japan (No. 2014-089).

ADDITIONAL INFORMATION

Supplementary information The online version contains supplementary material available at https://doi.org/10.1038/s41379-021-00910-x.

Correspondence and requests for materials should be addressed to Akihiko Yoshida.

Reprints and permission information is available at http://www.nature.com/reprints

Publisher's note Springer Nature remains neutral with regard to jurisdictional claims in published maps and institutional affiliations.